Supplementary Figure 1

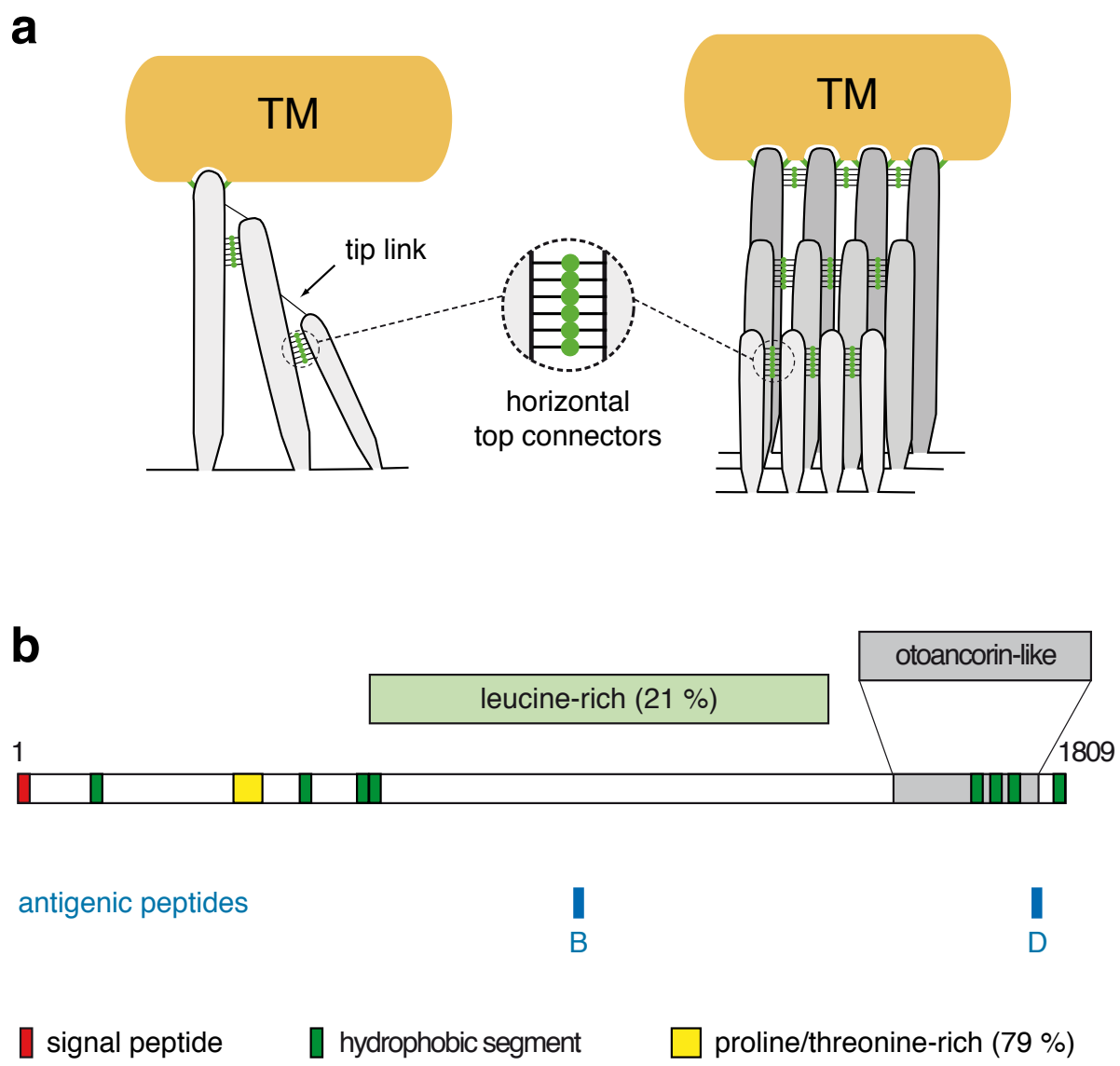

Supplementary Figure 1. (a) The outer hair cell's hair bundle (mouse). Stereocilia are arranged in three rows of graded heights. The tallest stereocilia have their tips anchored in the tectorial membrane (TM). The tip link extends from the tip of a stereocilium to the side of the adjacent taller one, and is thought to gate the mechanoelectrical transducer channel upon sound-induced deflection of the hair bundle. The horizontal top connectors connect the upper parts of adjacent stereocilia, both within and between rows. They have a zipper-like appearance, due to the presence of a central density (in green). **(b) Predicted structure of murine stereocilin and location of the antigenic peptides.** The sequences of stereocilin and otoancorin, defective in the DFNB16[4] and DFNB22[35] recessive forms of deafness, respectively, are 30 % identical in a 260/255 amino-acid fragment located in their C-terminal regions, i.e. aa 1507-1766 (stereocilin) and 831-1085 (otoancorin).

Supplementary Figure 2

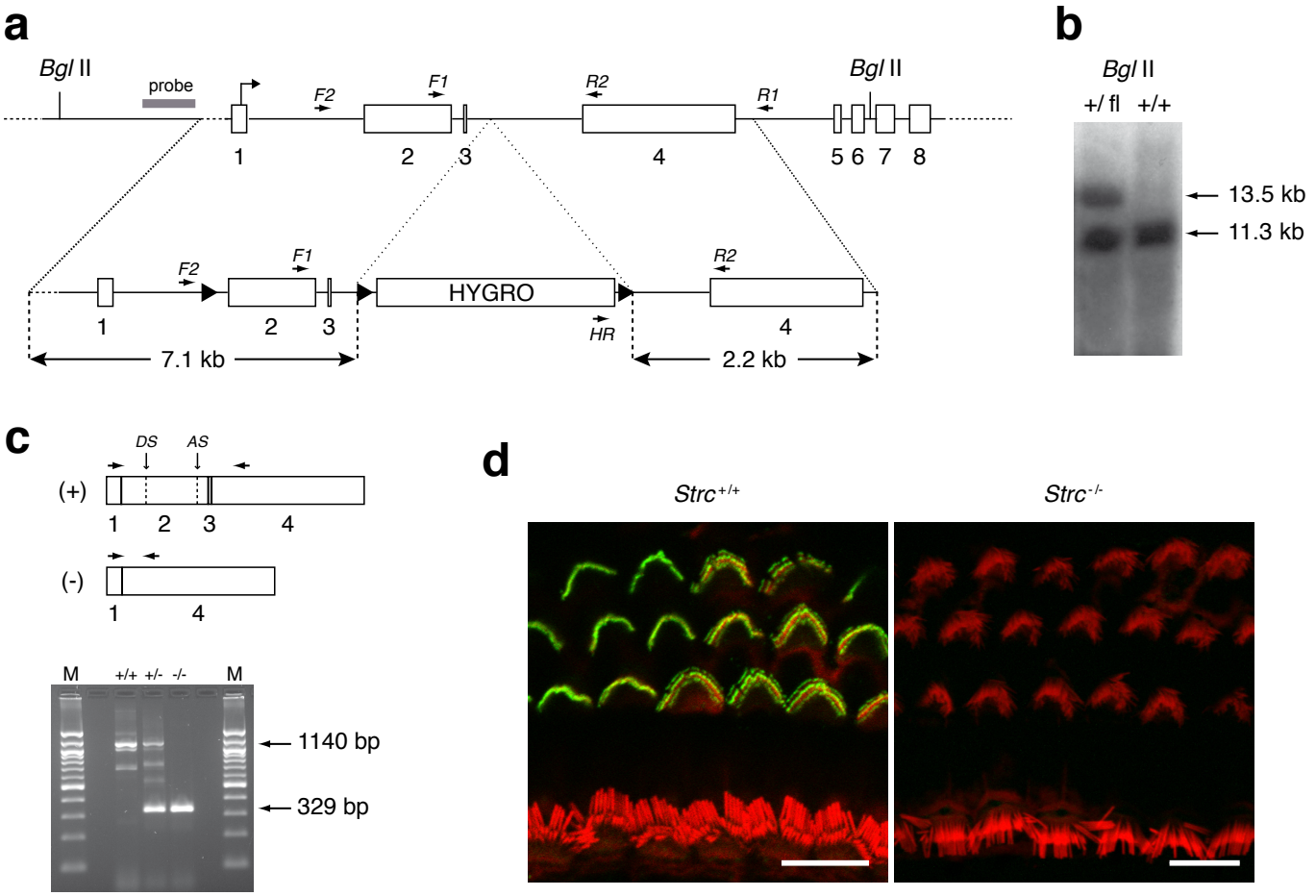

Supplementary Figure 2. Inactivation of the *Strc* gene. (**a**) Structure of the *Strc* 5' region and the targeting construct used to produce a floxed *Strc* allele with loxP sequences (triangles) flanking exons 2 and 3. Nucleotide primers used for PCR genotyping are indicated by arrows. (**b**) Southern blot of *Bgl* II-digested genomic DNA shows wild-type (+) and floxed (fl) *Strc* alleles. The probe hybridises to a 11.3 kb fragment from the wild-type allele and to a 13.5 kb fragment from the floxed allele carrying the hygromycin resistance gene. (**c**) RT-PCR analysis of *Strc* expression in $Strc^{+/+}$ (+/+), $Strc^{+/-}$ (+/-) and $Strc^{-/-}$ (-/-) P15 inner ears. The expected 1140 bp amplicon is seen in the +/+ and +/- lanes, together with products of lower molecular mass. Some of these products result from the use of alternative splice donor (DS, GT consensus at cDNA position 377) and acceptor (AS, AG consensus at cDNA position 827) sites located in exon 2. Some others are likely to correspond to heteroduplex molecules formed by different amplicons. The 329 bp amplicon from the deleted $Strc^{-/-}$ allele is present in the +/- lane and is the only product seen in the -/- lane. If translated, the $Strc^{-/-}$ allele, carrying the 811 bp frame shifting deletion of exons 2 and 3, would produce an incomplete signal peptide (19 out of 22 amino acids) followed by 30 out-of-frame amino-acids. M, 100 bp DNA ladder (Biolabs). (**d**) Compressions of z-stack confocal images of whole mount preparations of cochlear sensory epithelia from P14 $Strc^{+/+}$ and $Strc^{-/-}$ mice stained for stereocilin (green) and actin (red). The stereocilin labelling is detected in the $Strc^{+/+}$, but not $Strc^{-/-}$ cochlea. Scale bars : 10 μm.

Supplementary Figure 3

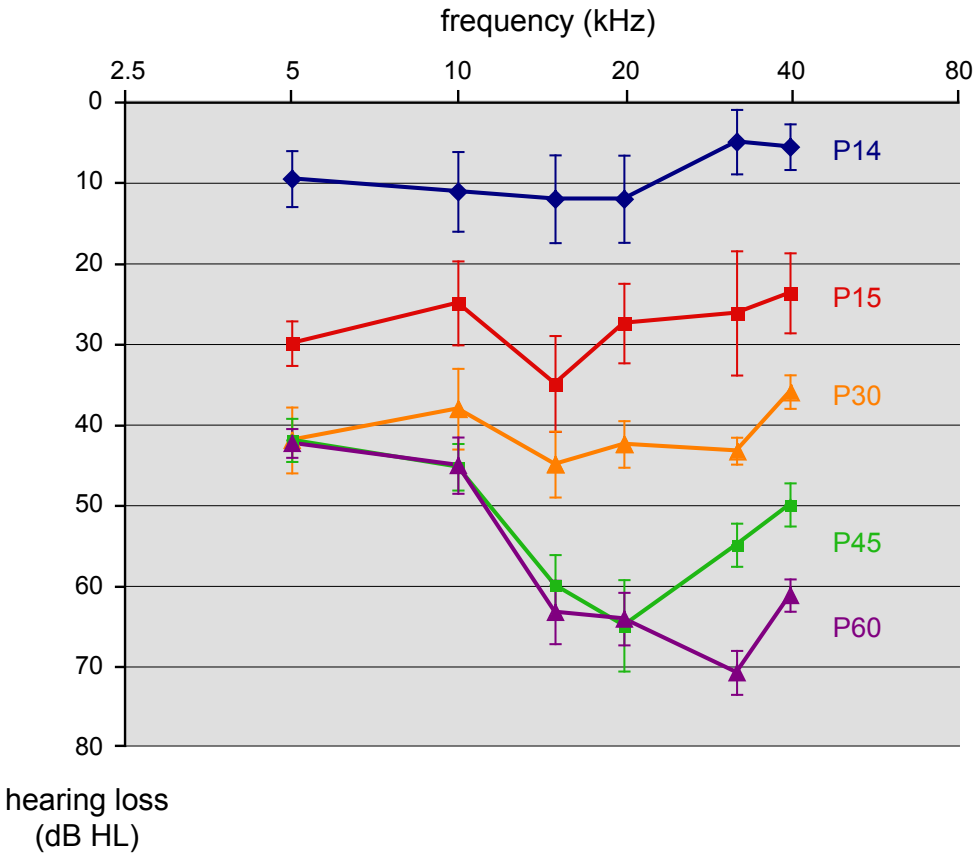

Supplementary Figure 3. Progressive elevation of hearing thresholds in *Strc*$^{-/-}$ mice.
To evaluate the effect of absent stereocilin on CAP thresholds in *Strc*$^{-/-}$ mice, the confounding effect of neural immaturity is removed by subtracting the CAP thresholds of age-matched *Strc*$^{+/+}$ mice at each postnatal stage. Thus at P14, the reference CAP audiogram was that represented on Fig. 1a (black line). At P15, the CAP audiogram of *Strc*$^{+/+}$ mice (grey line, Fig. 1b) was slightly more mature than at P14. From P30 on, the CAP audiogram of adult (P60) *Strc*$^{+/+}$ mice was used (Fig. 1b, black line). The resulting plots in dB HL -for Hearing Loss- (means ± one s.e.m.) reveal a progressive hearing loss in *Strc*$^{-/-}$ mice older than P14. With increasing age, the average hearing loss tends to that expected in case of total failure of the cochlear amplifier, that is 60 dB for sound frequencies above 10 kHz and about 40 dB at lower frequencies[16]. The progressive maturation of *Strc*$^{+/+}$ CAP audiograms with postnatal age matches that reported by Song *et al.* who report conspicuous maturation of the latencies and amplitudes of neural responses between P13 and P18[36].

Supplementary Figure 4

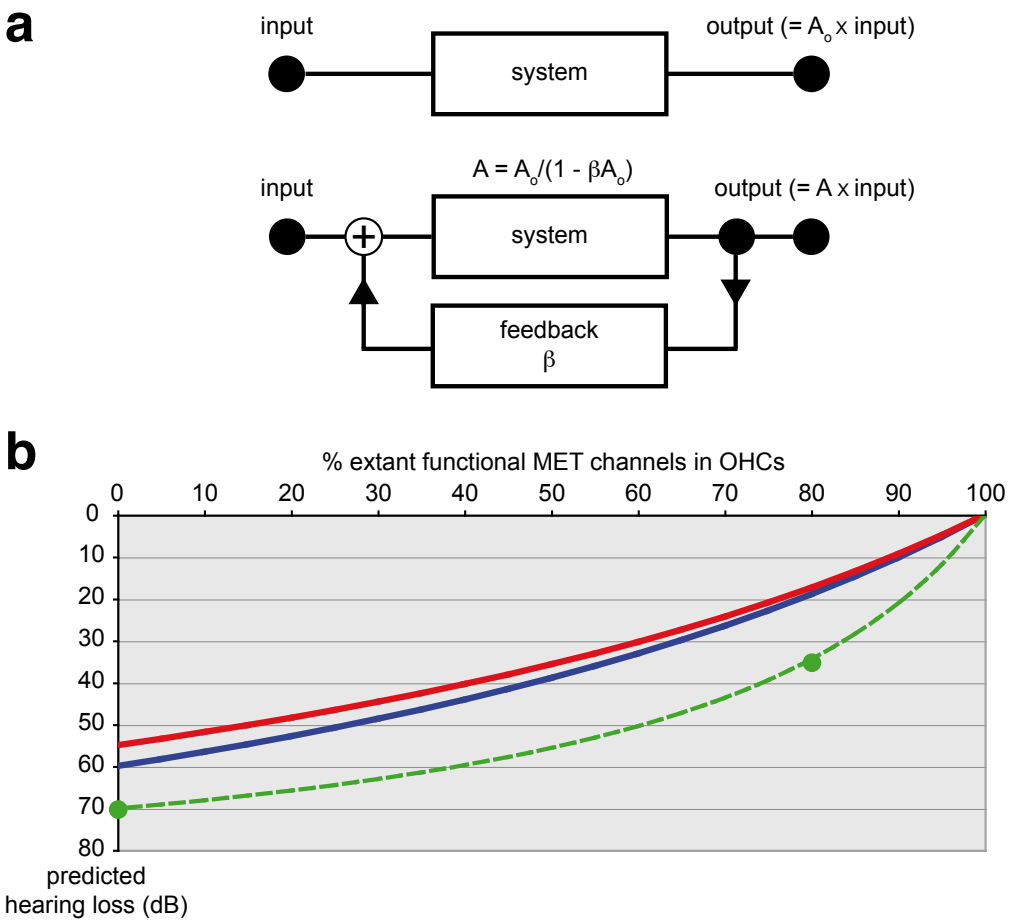

Supplementary Figure 4. Models of cochlear amplifier gain in relation to OHC-based electromechanical feedback. (a) Principle of a regenerative feedback amplifier. The gain A of a simple feedback-based amplifier (that is, the ratio output / input) is $A = A_0 / (1 - \beta A_0)$; A_0 is the gain in the absence of feedback (upper diagram), and β is the portion of the output that is fed back to the input of the system (lower diagram). If βA_0 is just slightly < 1, A is much larger than A_0 and the system possesses a large gain, ensuring high sensitivity. Tuning occurs as a result of feedback being effective only at the resonance frequency. **(b) Effect of decreased feedback strength.** Improved models account for the specifics of cochlear micromechanics[17,37]. They posit that β is proportional to the percentage n of functional MET channels in OHCs, and thus here, to the measured CM. The predicted hearing losses HL (in dB) due to decreased feedback strength exhibit similar shapes (red line, Patuzzi et al.[17], green dashed line, Neely & Kim[37], with the latter authors having solved the model exactly only at n = 0.8 and n = 0). The prediction used here (blue line) assumed a 60 dB gain at high sound frequencies, with HL given by[17]: HL = 60 (1 – n) / (1 – 0.46 n). To build Fig. 1c, experimentally estimated n's (from the % of extant low-frequency CM, black line in Fig. 1c) were fed into the formula giving HL (pink shaded area, Fig. 1c). For comparison, the observed hearing loss of *Strc*$^{-/-}$ mice (Fig. 1c, red line) was derived from averaging individual CAP thresholds across the 15-40 kHz frequency range, where CAP audiograms in dB HL were rather flat (supplementary Fig. 3), and where the normal gain is thought to be ~60 dB. Of note, the model predicts that the initial 20% drop in CM results in a ~20 dB-loss of gain. In contrast, the final 20% drop adds only ~7 dB to the already existing hearing loss (Fig. 1c). In between, i.e. from P15 to P45, the model also predicts the existence of residual gain and tuning. All these predictions were experimentally confirmed (Fig. 1c, 1e).

Supplementary Figure 5

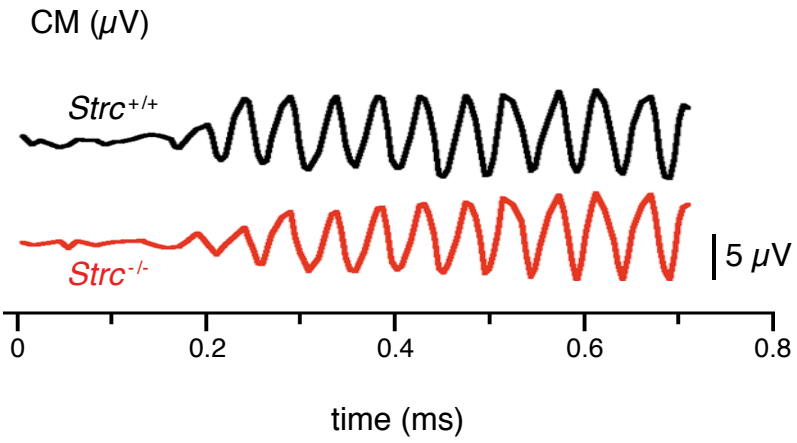

Supplementary Figure 5. Phase of CM response in *Strc*$^{+/+}$ and *Strc*$^{-/-}$ mice. CM responses to a 10 kHz tone burst at 60 dB SPL in one *Strc*$^{+/+}$ and one *Strc*$^{-/-}$ mouse at P14 show similar phases and onset times relative to the sound stimulus.

Supplementary Figure 6

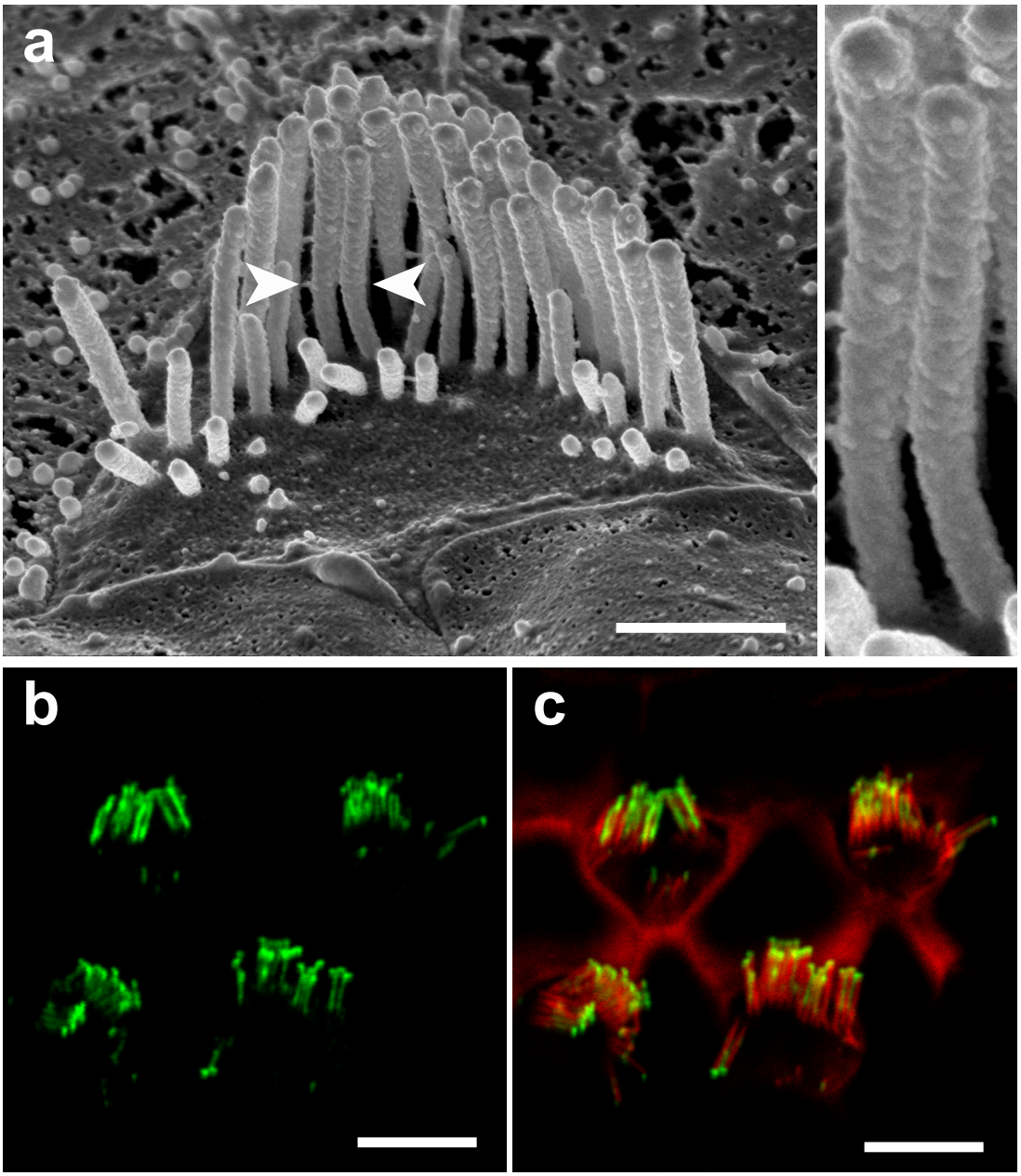

Supplementary Figure 6. Expanded distribution of stereocilin-associated lateral links and bending of adjacent stereocilia in harmonin-deficient (*Ush1c*$^{-/-}$) mice[38].

(**a**) Scanning electron micrograph of a mature *Ush1c*$^{-/-}$ OHC hair bundle. The lateral links extend further towards the stereocilia base, as best illustrated in one pair of stereocilia (arrowheads) on the corresponding two-fold enlargement (right panel). This results in a bending of adjacent stereocilia toward each other. (**b, c**) Single stack confocal images of mature *Ush1c*$^{-/-}$ OHC hair bundles stained for stereocilin (green, in b and c) and actin (red, in c). The stereocilin labelling between adjacent stereocilia distributes across the upper two thirds of the stereocilia length, instead of being restricted to a small distal region as in wild-type mice. Scale bars: 1 μm (a), 5 μm (b, c).

Supplementary Notes

35. Zwaenepoel, I. *et al*. Otoancorin, an inner ear protein restricted to the interface between the apical surface of sensory epithelia and their overlying acellular gels, is defective in autosomal recessive deafness DFNB22. *Proc. Natl. Acad. Sci. USA* **99**, 6240-6245 (2002).
36. Song, L., McGee, J. & Walsh, E. J. Frequency- and level-dependent changes in auditory brainstem responses (ABRS) in developing mice. *J. Acoust. Soc. Am.* **119**, 2242-2257 (2006).
37. Neely, S. T. & Kim, D. O. A model for active elements in cochlear biomechanics. *J. Acoust. Soc. Am.* **79**, 1472-1480 (1986).
38. Lefèvre, G. *et al*. A core cochlear phenotype in USH1 mouse mutants implicates fibrous links of the hair bundle in its cohesion, orientation and differential growth. *Development* **135**, 1427-1437 (2008).